Chapter IV

Discrete and 1D Polymeric Copper(II) Complexes of Tetranuclear Cubane-like Units: Structural and Magnetic Characterization

---

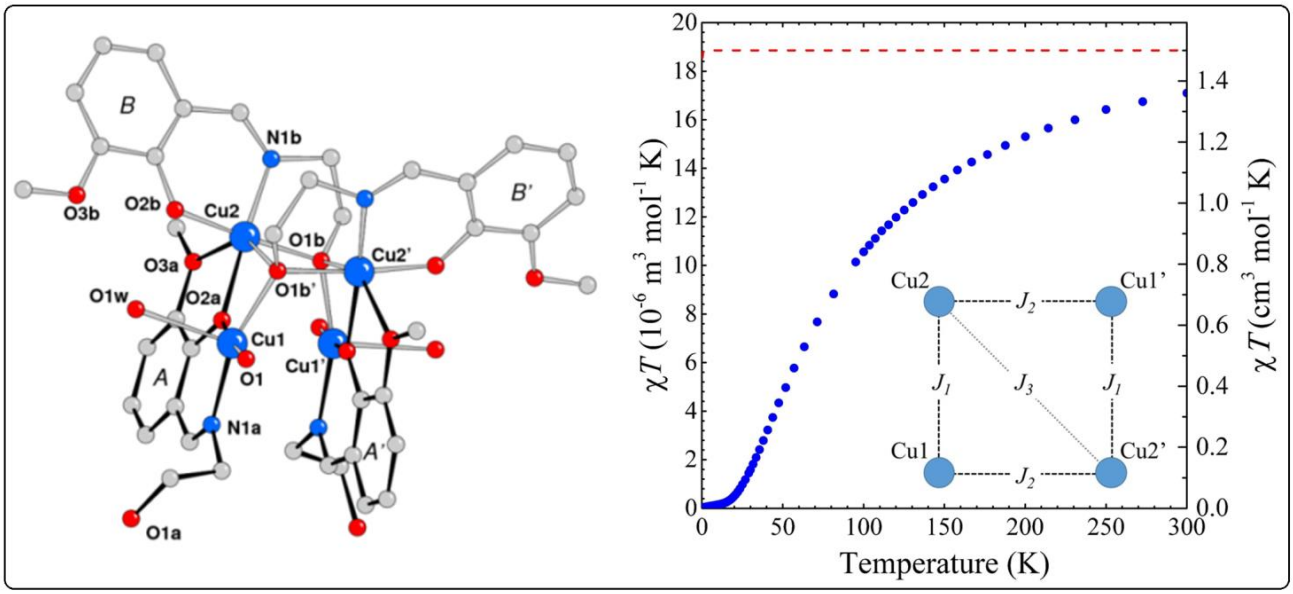

4.1. Introduction

The chemistry of polynuclear copper(II) complexes have attracted the interest of researchers not only for their peculiar structure, but also for potential applications in the area of magnetism,[4.1] bioinorganic chemistry,[4.2] and catalysis.[4.3] Multidentate amino alcohols are used for the synthesis of polynuclear copper(II) complexes adopting a self-assembly process. Since alcoholic hydroxyl groups can be easily deprotonated in presence of copper(II) ions, the resulting alkoxo moiety, acting as a bridging donor, can give rise to compounds of various nuclearity, from dimeric[4.4] to dinuclear,[4.5] trinuclear,[4.6] tetranuclear,[4.7] and hexanuclear,[4.8] copper(II) clusters, as well as coordination polymers. Multidentate Schiff bases derived from amino alcohols are often used to build polynuclear copper complexes since they can simultaneously act as chelating and bridging species towards the metal centres.[4.9]

Copper(II) complexes, especially those comprising a cubane-like Cu_4O_4 core, have been widely studied with the aim to synthesize magnetic materials,[4.10] a route favoured by possible different coordination geometries of the metal and the presence of unpaired electrons. Mergehenn and Haase have proposed a classification of cubane-like complexes considering the distribution of Cu−O distance values within the cube.[4.11-4.13] Thus, compounds having four long Cu−O distances between two pseudodimeric units have been classified of type I (displaying dominant antiferromagnetic interactions), while compounds with a pair of long distances within each of the pseudodimeric units have been classified of type II (displaying dominant ferromagnetic interactions). On the other hand, based on Cu···Cu distances Ruiz *et al.*[4.14] classified cubane compounds as: (i) [2+4], complexes with two short and four long Cu···Cu distances; (ii) [4+2], complexes with four short and two long Cu···Cu distances; (iii) [6+0], complexes with six equivalent Cu···Cu distances.

In the present contribution we have used a multidentate Schiff base ligand, 2-[(2-hydroxy-ethylimino)-methyl]-6-methoxy-phenol (H_2L) in combination of aromatic dicarboxylate species to synthesize copper complexes of double open cubane like core structure, $[Cu_4(L)_2(LH)_2(H_2O)_2]_2(NO_3)_2.(pydc).9H_2O$ (**1**) and $\{[Cu_4(L)_2(LH)_2(H_2O)_2(ppda)].5H_2O\}_n$ (**2**) (H_2L = 2-[(2-hydroxy-ethylimino)-methyl]-6-methoxy-phenol, pydc = pyridine-3,5-dicarboxylate, ppda = phenylene-1,4-diacrylate). Variable temperature magnetic properties of the complexes have been studied.

4.2. Experimental

4.2.1. Materials and Physical Measurements

Highly pure ethanolamine (98%) was purchased from Merck. All other starting materials were commercially available reagent grade and used as received. Solvents used for spectroscopic studies were purified and dried by standard procedures before use.[4.15]

Elemental analyses (carbon, hydrogen and nitrogen) were performed using a Perkin–Elmer 240C elemental analyzer. Electronic absorption spectra were obtained with a Shimadzu UV-1601 UV–Vis spectrophotometer at room temperature. Quartz cuvettes of 1 cm path length and 3 cm^3 volume were used for all measurements. IR spectra were recorded as KBr pellets on a Bruker Vector 22 FTIR spectrophotometer operating from 400 to 4000 cm^{-1}. Emission spectra were recorded in methanolic solution on a Hitachi F-7000 spectrofluorimeter using a quartz cell of 1 cm path length at room temperature (300 K). Quantum yield was calculated according to the reported method.[4.16] Electrochemical measurements were done by a BAS Epsilon electrochemical system under dry argon atmosphere. A three-electrode assembly comprising a glassy carbon (for reduction) or Pt (for oxidation) working electrode, Pt auxiliary electrode, and an aqueous Ag/AgCl reference electrode were used.

Magnetic measurements

The low-field magnetic susceptibility and magnetization were measured using a Quantum Design Magnetic Properties Measurement System. The magnetic moment was measured using the DC SQUID option, where for each measurement the sample is moved through four compensated superconducting pickups coils that are in the "second derivative" configuration, coupled to an rf SQUID.[4.17] The moment is deduced by a fit to the observed voltage, which is proportional to the flux sum through the magnetometer coils. The magnetic moment was measured in temperature range from 1.8 to 300 K, at a constant field of 0.1 T. The magnetization as function of field was also measured, at 1.8, 4.2 and 10 K.

For the polycrystalline compounds **1**, the samples were measured whilst held in a small gelatin capsule. For compound **2**, a stack of two single crystals were used, with the applied magnetic field normal to the crystal planes. The crystals were held together with a thin layer of Apiezon N grease.

Diamagnetic corrections (-1.552×10^{-8} m^3/mol for complex **1** and -8.552×10^{-9} m^3/mol for **2**) were calculated from standard tables and have been removed from the data.

4.2.2. Synthesis

Complexes **1** and **2** are schematically displayed in Scheme 4.1 with indication of the procedures adopted for their synthesis.

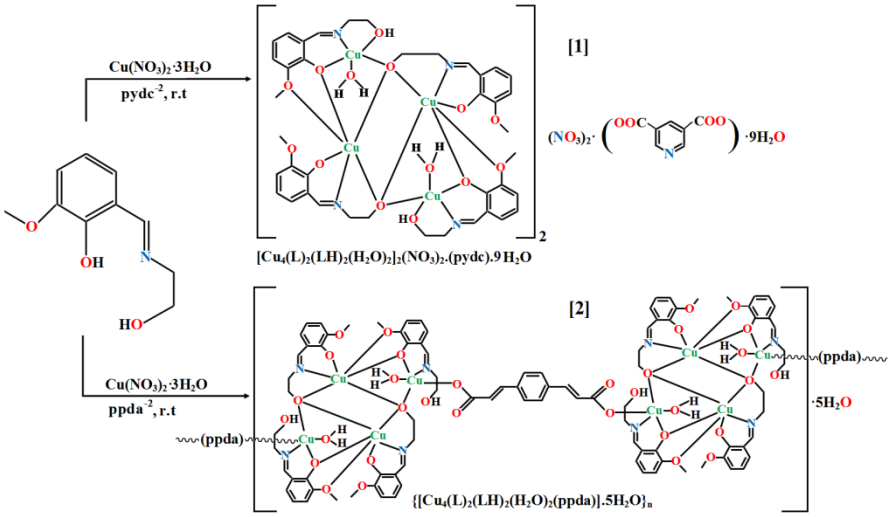

Scheme 4.1. Synthesis of 1-2.

4.2.2.1. Synthesis of ligand

The ligand H_2L, 2-[(2-hydroxy-ethylimino)-methyl]-6-methoxy-phenol was synthesized by stirring a methanolic solution of 3-methoxysalicyldehyde (1 mmol, 0.152 g) and 2-aminoethanol (1 mmol, 0.061 g) at room temperature. The ligand was directly used for the preparation of the compounds.

4.2.2.2. Synthesis of the Complexes 1 and 2

Synthesis of $[Cu_4(L)_2(LH)_2(H_2O)_2]_2(NO_3)_2.(pydc).9H_2O$ (1)

A methanolic solution (10 mL) of mixture of 2-[(2-hydroxy-ethylimino)-methyl]-6-methoxy-phenol (H_2L) (0.5 mmol, 0.0976 g) and Et_3N (0.5 mmol, 0.05 g) was added to a methanolic solution of $Cu(NO_3)_2.3H_2O$ (0.5 mmol, 0.120 g) and stirred for 1h. Then, a methanolic solution (10 mL) of pyridine 3,5-dicarboxylic acid (0.5 mmol, 0.83 g) and Et_3N (1 mmol, 0.10 g) was added dropwise and stirred for additional 2 h, and filtered. The filtrate was kept at room temperature and deep green crystals suitable for X-ray diffraction were obtained after a few days. Yield: 60%. Anal. Calcd for $C_{87}H_{121}Cu_8N_{11}O_{47}$ (2581.27g mol^{-1}): C, 40.48; H, 4.72; N, 5.96. Found: C, 40.50; H, 4.74; N, 5.94.

Synthesis of $\{[Cu_4(L)_2(LH)_2(H_2O)_2(ppda)].5H_2O\}_n$ (2)

Complex **2** was synthesised adopting same procedure as for complex **1**, using phenylene-1,4-diacrylic acid (0.5 mmol, 0.109 g) instead of pyridine-3,5-dicarboxylic acid. Yield: 65%. Anal. Calcd for $C_{52}H_{68}Cu_4N_4O_{23}$ (1371.26 g mol^{-1}): C, 45.54; H, 4.99; N, 4.08. Found: C, 45.56; H, 5.01; N, 4.06.

4.2.3. Crystallographic Data Collection and Refinement

Data collection for complexes **1**-**2** were carried out at 100 K and 120 K, respectively, with Mo-Kα radiation (λ = 0.71073 Å) on a Xcalibur diffractometer, equipped with Sapphire 3CCDcamera. Cell refinement, indexing and scaling of the data sets were done by using program CrysAlisPro.[4.18a] The structures were solved by direct methods and subsequent Fourier analyses[4.18b] and refined by the full-matrix least-squares method based on F^2 with all observed reflections.[4.18b] In the crystal of **1** one lattice water was refined over two positions with occupancies 0.632(14)/0.368(14). The uncoordinated ethanol chain in **2** was found disordered over two positions with refined occupancy of 0.74(1)/0.26(1). Moreover in **2** an occupancy of 0.50, 0.50, 0.30, 0.20, was assigned to four water molecules (H atoms not assigned for the latter two) based on the respective peak height of the Fourier map. Hydrogen atoms were placed at calculated positions, except those of water molecules, which were detected on the difference Fourier map, and refined with restraints on O-H bond length (0.85 Å). All the calculations were performed using the WinGX System, Ver 1.80.05.[4.18c] Molecular structures were done with graphical program Diamond.[4.18d] Crystal data and details of refinements are given in Table 4.1.

Table 4.1. Crystal data and details of structure refinement for compounds 1 and 2.

Complex	1	2
Empirical formula	$C_{87}H_{121}Cu_8N_{11}O_{47}$	$C_{52}H_{68}Cu_4N_4O_{23}$
Formula mass, g mol^{-1}	2581.27	1371.26
Crystal system	Monoclinic	Monoclinic
Space group	$P2_1/c$	$P2/n$
a, Å	24.0049(4)	10.9272(3)
b, Å	24.3725(4)	14.8744(4)
c, Å	18.2532(4)	17.5243(4)
β, deg	101.556(2)	98.084(2)
V, Å^3	10462.7(3)	2820.02(13)
Z	4	2
$D_{(calcd)}$, g cm^{-3}	1.629	1.615
μ(Mo-Kα), mm^{-1}	1.692	1.573
F(000)	5312	1416
Theta range, deg	2.51 - 27.88	2.98 - 27.70
No. of collected data	94532	18168
No. of unique data	24388	6127
R_{int}	0.0876	0.0535
Observed reflns [$I > 2\sigma(I)$]	15322	3826
Goodness of fit (F^2)	1.021	1.020
Parameters refined	1404	393
$R1$, $wR2$ ($I > 2\sigma(I)$) [a]	0.0673, 0.1327	0.0606, 0.1027
Residuals, e Å^{-3}	1.510, –1.454	1.000, –0.647

4.3. Results and discussion

4.3.1. Molecular structure of complexes

The Schiff base ligand H_2L used in the synthesis of the present complexes was obtained upon condensation of 3-methoxysalicylaldehyde and ethanolamine. The ligand H_2L in principle can behave as tetradentate, but here it acts as tri- as well as tetra- coordinating species.

The structural analysis of complex **1** revealed that the crystallographic independent unit comprises two tetranuclear cationic species, of which one is shown in Figure 4.1 (the other cation is reported in Figure 4.2), counter balanced by one 3,5-pyridinedicarboxylate and two nitrate anions beside a different amount of lattice water molecules. The coordination bond lengths are reported in Table 4.2. Being the two independent complex units close comparable, the description is limited to one of these.

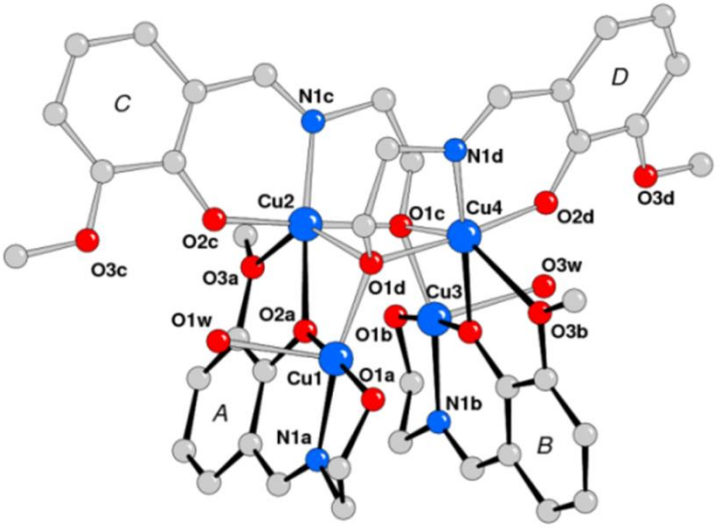

Figure 4.1. Molecular structure of one of the two independent complex cations (A) of 1 with labels of heteroatoms.

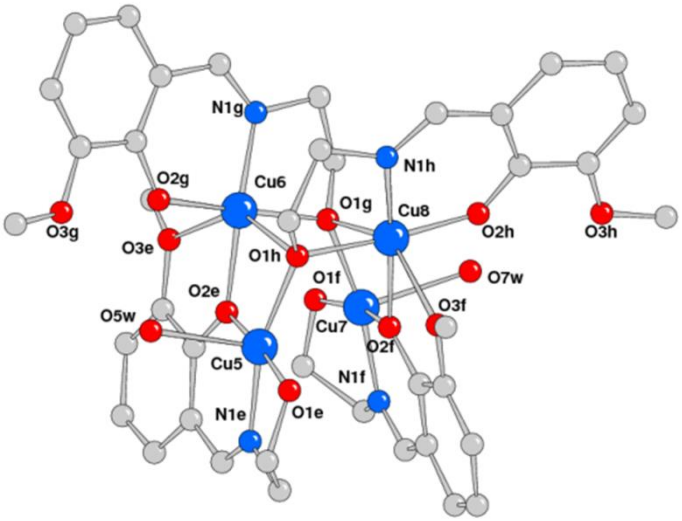

Figure 4.2. Molecular structure scheme of the complex cation B of 1 with labels of heteroatoms.

Table 4.2. Coordination bond distances [Å] for the two complex cations of 1.

Cation A		Cation B	
Cu(1)-N(1a)	1.946(4)	Cu(5)-N(1e)	1.931(5)
Cu(1)-O(1a)	2.012(4)	Cu(5)-O(1e)	2.001(4)
Cu(1)-O(2a)	1.942(3)	Cu(5)-O(2e)	1.950(3)
Cu(1)-O(1d)	1.936(3)	Cu(5)-O(1h)	1.929(3)
Cu(1)-O(1w)	2.266(3)	Cu(5)-O(5w)	2.295(4)
Cu(2)-N(1c)	1.929(4)	Cu(6)-N(1g)	1.932(4)
Cu(2)-O(1c)	1.978(3)	Cu(6)-O(1g)	1.958(3)
Cu(2)-O(2c)	1.914(3)	Cu(6)-O(2g)	1.902(3)
Cu(2)-O(2a)	1.985(3)	Cu(6)-O(2e)	1.985(3)
Cu(2)-O(3a)	2.386(4)	Cu(6)-O(3e)	2.474(4)
Cu(2)-O(1d)	2.538(4)	Cu(6)-O(1h)	2.431(3)
Cu(3)-N(1b)	1.939(4)	Cu(7)-N(1f)	1.931(5)
Cu(3)-O(1b)	2.025(4)	Cu(7)-O(1f)	2.005(4)
Cu(3)-O(1c)	1.942(3)	Cu(7)-O(1g)	1.923(3)
Cu(3)-O(2b)	1.936(3)	Cu(7)-O(2f)	1.954(3)
Cu(3)-O(3w)	2.255(4)	Cu(7)-O(7w)	2.269(4)
Cu(4)-N(1d)	1.941(4)	Cu(8)-N(1h)	1.922(4)
Cu(4)-O(1d)	1.974(3)	Cu(8)-O(1h)	1.967(3)
Cu(4)-O(2d)	1.921(3)	Cu(8)-O(2h)	1.903(3)
Cu(4)-O(2b)	1.986(3)	Cu(8)-O(2f)	1.993(3)
Cu(4)-O(3b)	2.419(4)	Cu(8)-O(3f)	2.419(4)
Cu(4)-O(1c)	2.419(4)	Cu(8)-O(1g)	2.560(3)

As can be noted from Figure 4.1, the complex is characterized to contain a distorted cubane-type core and consists of four copper(II) centres coordinated by two monodeprotonated $[HL]^{-}$, two dideprotonated $[L]^{2-}$ ligands, and two water molecules. Each monodeprotonated ligand (A, B rings in Figure 4.1) chelates two copper atoms *via* μ_2-η^2:η^2-*O, O, N, O* coordination mode, while the double deprotonated ones (phenolate rings C, D) chelate Cu2 and Cu4, and in addition connect the previous moieties with the μ_3-alkoxido group, while the methoxy oxygens O3c and O3d remain uncoordinated (μ_3-η^1:η^1:η^3-*O, N, O* coordination mode). The pair of ligands A/B and C/D are arranged in a head-tail fashion about the cubane-like core so that the complex presents a pseudo two-fold axis passing in between Cu2/Cu4 and Cu1/Cu3.

The Schiff base mean planes through A/B and C/D form a dihedral angle of ca. 31.0 and 42.0°, respectively.

Figure 4.3 shows a simplified representation of the coordination environment around the four metal centres. The metal ions Cu1 and Cu3 present a similar square pyramidal geometry, being chelated by the imine nitrogen, the phenoxido and the alcoholic oxygen of one monodeprotonated ligand and complete the basal plane with the alkoxido oxygen (μ_3-bridging species) from a double deprotonated ligand. A water molecule is located at apical position of the coordination sphere. The basal coordination bond distances for Cu1 and Cu3 (Table 4.2) are in between 1.936(3)-2.025(4) Å, and the slight longer values refer to the alcoholic oxygen atoms O1a and O1b. The aqua ligand at the apical position is somewhat more distant, being at 2.266(3) and 2.255(4) Å for Cu1 and Cu3, respectively. On the other hand, Cu2 and Cu4 show a distorted octahedral coordination sphere achieved by the imine nitrogen, the phenoxido and the alkoxido oxygen from one $[L]^{2-}$ ligand, and at axial positions by a second alkoxido and a methoxy oxygen from two other Schiff bases. The equatorial bond distances fall in the range 1.914(3)-1.986(3) Å, while the axial bond lengths vary from 2.386(4) to 2.538(4) Å due to the Jahn-Teller distortion. As a matter of fact the metals are located at the vertices of a distorted tetrahedron with edge dimension varying from 3.1482(9) to 3.3976(9)Å, with the exception of Cu1···Cu3 distance of 3.9385(9) Å, which is the longest. As result of an extended H-bonding scheme the lattice water molecules, nitrate and py-3,5-dicarbixylate ions form layers (depicted in Figure 4.4), which sandwich the tetranuclear complexes and give rise to a 3D network through additional hydrogen bonds.

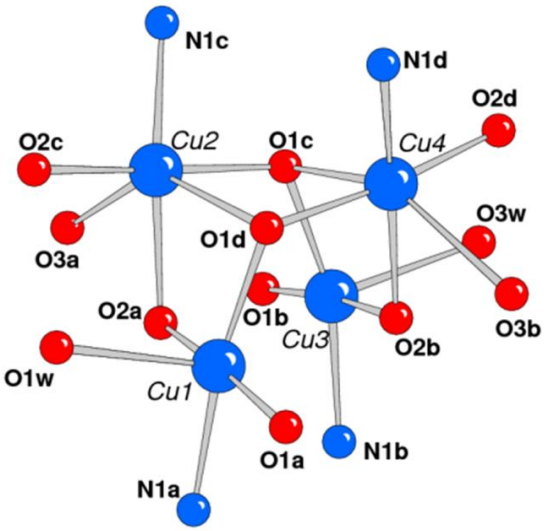

Figure 4.3.The distorted cubane-like core of complex 1.

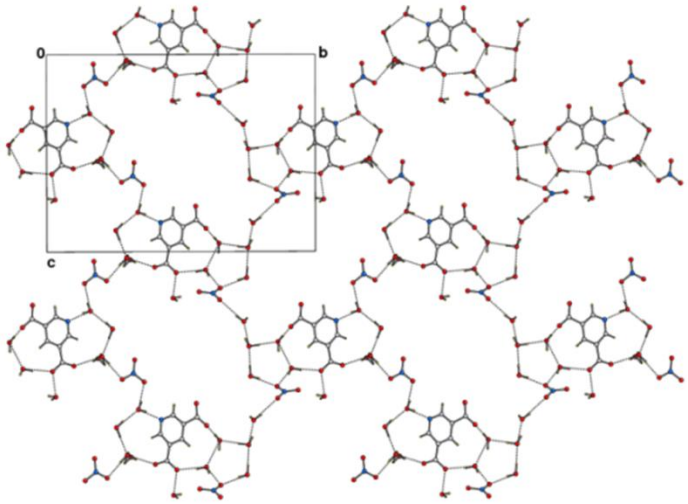

Figure 4.4. Layered structure of compound 1 formed by nitrate, 3,5-dicarboxylate pyridine and water molecules connected by H-bonds.

Complex **2** is a 1D coordination polymer (Figure 4.5), developed along the [101] direction, in which the tetranuclear copper units are connected by the *p*-phenylenediacrylate anions ($ppda^{-2}$) as shown in Figure 4.6. The tetranuclear cubane-like core is close comparable to the cations observed for complex **1** (as evident by comparing Figures 4.6 and 4.1), but it is located on a crystallographic two-fold axis, and thus only two copper atoms, Cu1 and Cu2, are crystallographically independent. However in the present case, the formation of the chain is allowed by the different coordination mode (μ_2-η^2:η^1-*O, O, N*) of the monodeprotonated $[HL]^-$ ligand (A in Figure 4.6) being the alcoholic -CH_2-CH_2-OH group uncoordinated. On the other hand the dideprotonated $[L]^{2-}$ ligand (B) maintains the same coordination mode as

observed in the discrete complexes of **1**. The coordination distances for the penta- and hexa-coordinated Cu1 and Cu2 atoms, respectively (Table 4.3) evidence a trend similar as for complex **1**. The apical Cu1-O1w bond length, of 2.361(3) Å, is longer with respect to the basal distances, varying from 1.948(3) to 1.972(4) Å. On the otherhand the axial distances of octahedral Cu2, of 2.388(3) and 2.400(3) Å, are significantly longer than the equatorial ones that fall in the range 1.910(3)-1.996(3)Å. The edges of the tetrahedral Cu_4 metal unit present an extended distance (Cu(1)···Cu(1') = 3.9323(11) Å) over the other values (range 3.1399(12)-3.3876(8) Å). The coordination polymers interdigitate in such a way that the crystal packing shows series of alternating hydrophobic and hydrophilic regions, the latter clustering the lattice water molecules (some of low occupancy) connected by H-bonds (Figure 4.7).

Table 4.3. Coordination bond distances [Å] for 2.

Cu(1)-O(2a)	1.948(3)	Cu(2)-O(2b)	1.910(3)
Cu(1)-O(1)	1.961(3)	Cu(2)-N(1b)	1.936(4)
Cu(1)-O(1b')	1.971(3)	Cu(2)-O(1b)	1.971(3)
Cu(1)-N(1a)	1.972(4)	Cu(2)-O(2a)	1.996(3)
Cu(1)-O(1w)	2.361(3)	Cu(2)-O(3a)	2.388(3)
		Cu(2)-O(1b')	2.400(3)

[#]Only the crystallographically independent values are reported. Primed atoms at –x+1/2, y,–z+3/2

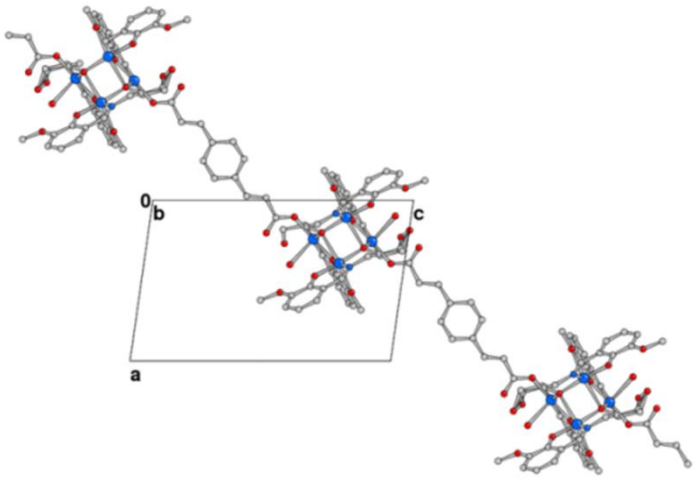

Figure 4.5. 1D coordination polymer of 2 viewed down b axis.

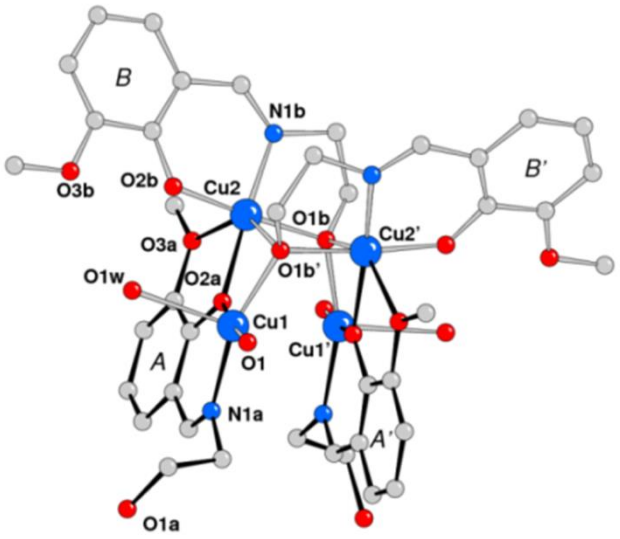

Figure 4.6. Molecular structure of the tetranuclear unit for complex 2, located on a crystallographic two- fold axis. Atom O1 represents the carboxylic oxygen of the bridging phenylenediacrylate anion.

The same Schiff base ligand or its *p*-bromoderivative has been used for the construction of exa- and epta-iron complexes,[4.19] heterometallic nonanuclear species Na_2Mn_6Ln (Ln = Eu, Gd, Tb, Dy)[4.20] and also of tetranuclear Ni_4 complexes.[4.21] Of these, the latter discrete complexes have structural features similar to those of complex **2**, being oxygen atoms O1 of the bridging phenylenediacrylate replaced by monocoordinated NCSe or NCS anions. In addition the phenolate A/A' rings (Figure 4.6) are closer so that to accomplish an octahedral coordination for all the Ni atoms. Thus the formation of polymeric species for these complexes becomes feasible for the different coordination mode of the ligands about the tetranuclear metal core and it is likely that for steric reasons only long bridging spacers like *p*-phenylenediacrylate allows the formation of observed chains.

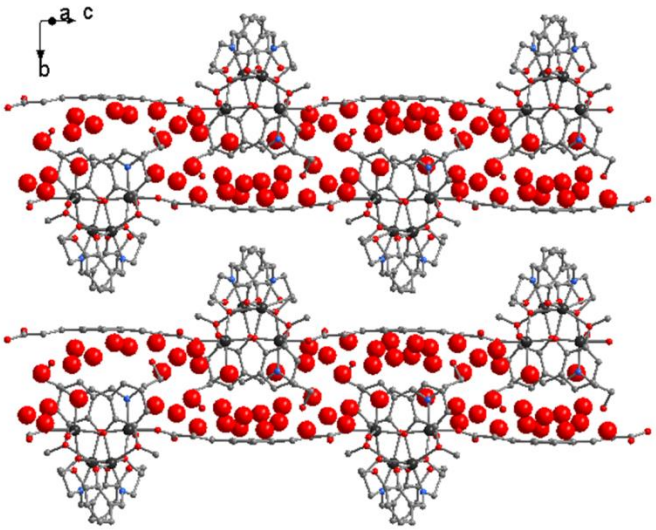

Figure 4.7. Crystal packing of complex 2 highlighting the position of the lattice molecules.

Table 4.4. Intermetallic distances [Å] for the two complex cations of 1.

Cation A		Cation B	
Cu(1)-Cu(2)	3.1520(9)	Cu(5)-Cu(6)	3.1461(9)
Cu(1)-Cu(3)	3.9385(9)	Cu(5)-Cu(7)	3.8495(9)
Cu(1)-Cu(4)	3.3976(9)	Cu(5)-Cu(8)	3.3268(8)
Cu(2)-Cu(3)	3.3450(8)	Cu(6)-Cu(7)	3.3973(9)
Cu(2)-Cu(4)	3.3114(9)	Cu(6)-Cu(8)	3.2509(8)
Cu(3)-Cu(4)	3.1482(9)	Cu(7)-Cu(8)	3.1899(8)

Table 4.5. Intermetallic distances [Å] for 2.

Cu(1)-Cu(2)	3.1913(7)	Cu(1)-Cu(1')	3.9323(11)
Cu(1)-Cu(2')	3.3876(8)	Cu(2)-Cu(2')	3.1399(12)

Primed atoms at -x+1/2,y,-z+3/2

4.3.2. Electronic absorption and emission spectra of complexes 1 and 2

The electronic absorption spectra of two complexes have been recorded in methanol at concentration 1.651×10^{-5} mM (Figure 4.8). Complex **1** shows significant transitions at 209 nm ($\varepsilon \sim 1.61\times 10^{7}$ L M^{-1} cm^{-1}), 231 nm ($\varepsilon \sim 1.21\times10^{7}$ L M^{-1} cm^{-1}), 270 nm ($\varepsilon \sim 5.26\times10^{6}$ L M^{-1} cm^{-1}) and 373 nm ($\varepsilon \sim 6.66\times10^{5}$ L M^{-1} cm^{-1}) and for complex **2** transitions are at 234 nm ($\varepsilon \sim 4.11\times 10^{6}$ L M^{-1} cm^{-1}), 277 nm ($\varepsilon \sim 2.36\times10^{6}$ L M^{-1} cm^{-1}), 327 nm ($\varepsilon \sim 1.27\times10^{6}$ L M^{-1} cm^{-1}), 370 nm ($\varepsilon \sim 6.05\times10^{5}$ L M^{-1} cm^{-1}).

On excitation at 270 nm, complex **1** exhibits luminescence bands at 313, 361 nm in methanol at room temperature and complex **2**, on excitation on 277 nm, exhibits luminescence bands at 313, 329, 357 nm (Figure 4.9).

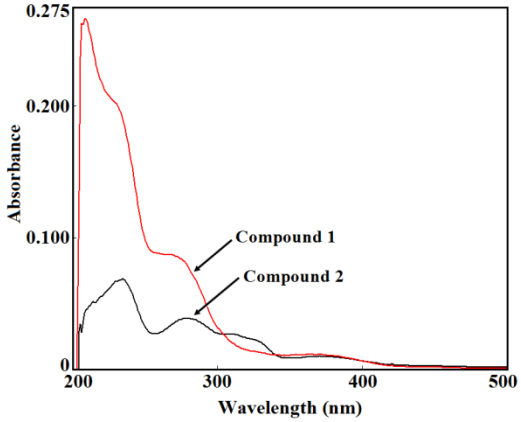

Figure 4.8. Absorption spectra of complexes 1(red) and 2 (black).

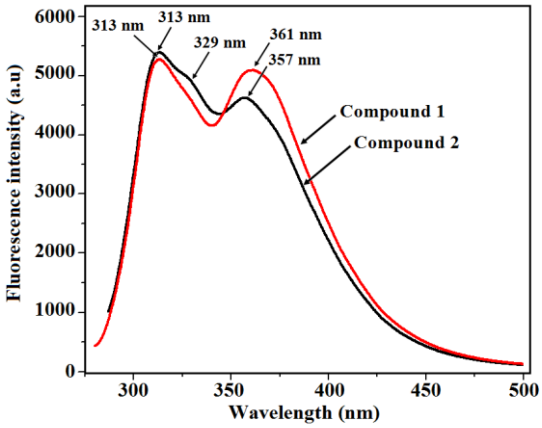

Figure 4.9. Emission spectra of complexes 1(red) and 2 (black).

4.3.3. FTIR spectra of complexes 1 and 2

The IR spectra show a broad band around 3425 cm^{-1} for complex **1**, and 3415 cm^{-1} for complex **2**, which are assigned to the ν(OH) stretching vibration of the lattice water molecules (Figure 4.10). In addition bands at 506, 814 cm^{-1} for complex **1**, and 509, 814 cm^{-1} for complex **2** indicate the presence of coordinated water molecules.[4.22] The bands at 1429 cm^{-1} (for **1**) and 1425 cm^{-1} (for **2**) are due to the azomethine (C=N) group. The sharp peak at 1370 cm^{-1} for complex **1** gives evidence for the presence of free nitrate ion.[4.22] The bands at 2972 cm^{-1} (for **1**) and 2975 cm^{-1} (for **2**) are due to aromatic C-H stretching vibration; bands at

2940 cm^{-1} (for **1**) and 2943 cm^{-1} (for **2**) correspond to aliphatic *ν*(C-H) stretching vibration. Bands at 1124 cm^{-1} and 1166 cm^{-1} for **1** and **2**, respectively, were assigned to *ν*($O–CH_3$) stretching vibrations.

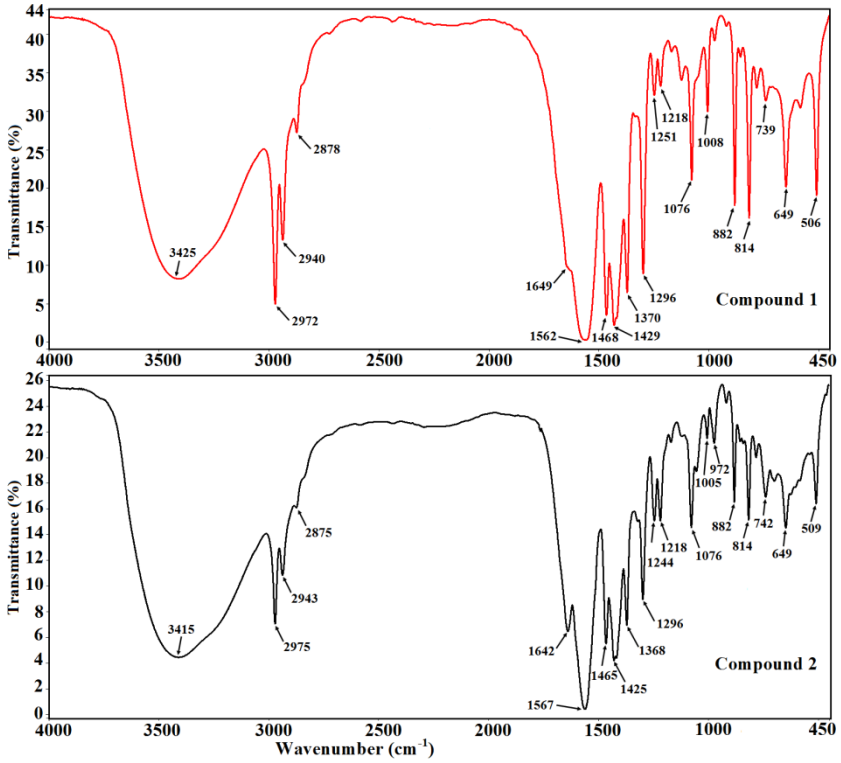

Figure 4.10. IR spectrum of complexes 1 (red) and 2 (black).

4.3.4. Magnetic properties of complexes

Figures 4.11 and 4.12 show the low-field magnetic susceptibility χ *vs* temperature *T* plots for compounds **1** and **2**. Plots of χT *vs* T, displayed in Figures 4.13 and 4.14, reveal that in both cases χT decreases on decreasing temperature, indicating that the materials are dominated by antiferromagnetic behaviour throughout the temperature range of the measurements. Moreover, in both complexes χT begins to approach saturation at high temperatures in good agreement with the values expected for a system of completely independent Cu(II) spins assuming a *g*-factor of 2, as shown by the dotted lines indicated in Figures 4.13 and 4.14.

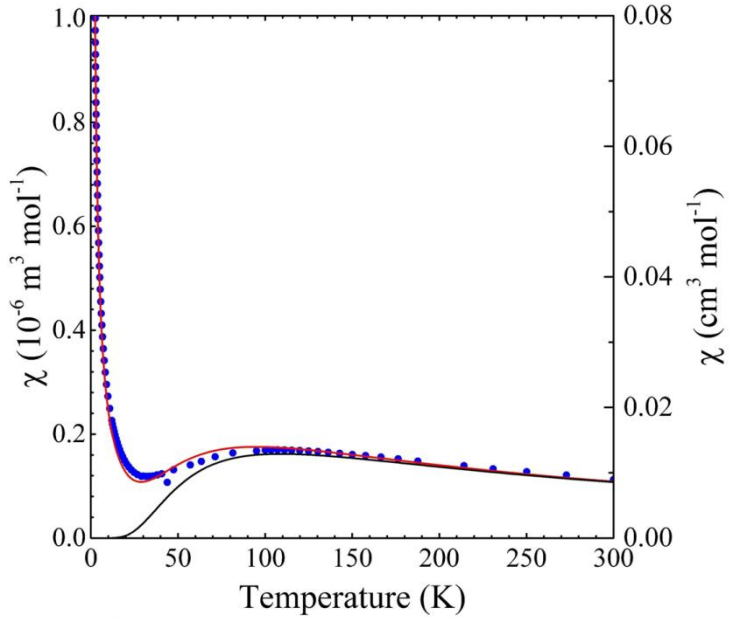

Figure 4.11. Plot of magnetic susceptibility χ as function of temperature for complex 1 at 0.1 T. The black line represents the model described in the text assuming no free moments, the red line includes a small number of independent *s*=1/2 spins (left-hand scale in SI units and right-hand scale in CGS units).

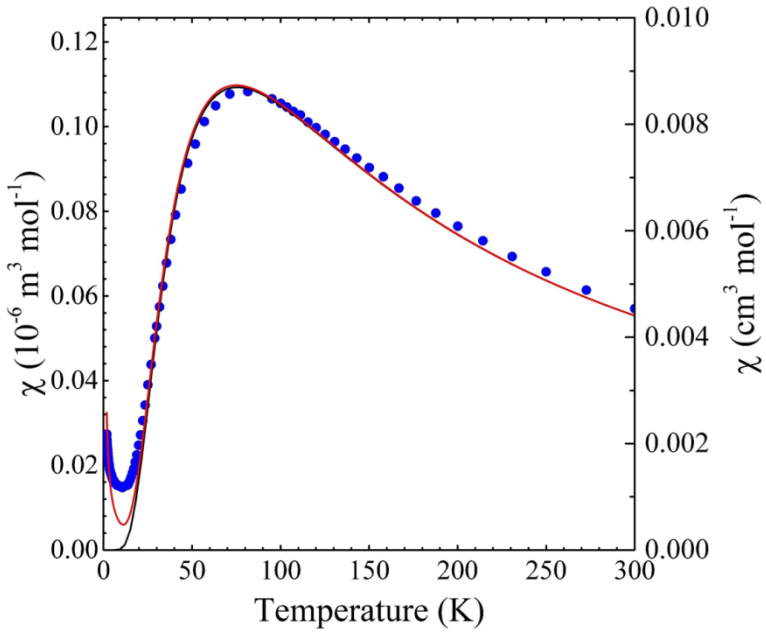

Figure 4.12. Plot of magnetic susceptibility χ as function of temperature for complex 2 at 0.1 T. The black line represents the model described in the text assuming no free moments, the red line includes a small number of independent *s*=1/2 spins. Data were taken with field normal to the crystal planes (left-hand scale in SI units and right-hand scale in CGS units).

The plots of χ *vs* the temperature (Figures 4.11 and 4.12) for both materials exhibit a broad hump as temperature is lowered, the position of which is related to the strength of the effective antiferromagnetic exchange in the system. The hump occurs near 100 K for complex **1** and at 75 K for **2**. Both data sets show an upturn in susceptibility at the lowest

temperatures. This feature is frequently observed in Cu(II) cubane complexes[4.23] and is typically attributed to a small amount of paramagnetic impurities. Alternatively, spin vacancies in the cubane-like structures would give rise to magnetic moment uncoupled to a nearer neighbour and could lead to a paramagnetic response at low temperatures too. We also noted that inequivalent spins within each unit cell have coordination environments, and hence *g*-tensors, that are not co-aligned. In the zig-zag Cu(II) chains, a staggering of *g*-tensors within each unit cell is known to result in a paramagnetic-like upturn in susceptibility as temperature is lowered.[4.24]

Both the complexes **1** and **2** have a distorted doubly-open cubane structure in which pairs of Cu(II) ions are linked via one or two Cu-O-Cu bonds. The corresponding bond angles, analyzed via the Goodenough-Kanamori-Anderson rules[4.25] are consistent with an antiferromagnetic exchange suggested from the χT plots. Using data of Table 4.6, a schematic cubane-like core of complex **2** can be constructed as shown in Figure 4.15(a). This indicates that bonds in Cu1-O2a-Cu2 are shorter than in Cu1-O1b'-Cu2 with a larger angle for the former fragment; hence this pathway is expected to provide the strong antiferromagnetic interaction between these spins. Similarly is observed for Cu1' and Cu2' for symmetry. Thus there is a similar pathway between Cu1 and Cu2' (and Cu1' and Cu2) via O1b' (O1b). However, the length of this pathway and the lack of significant orbital overlap in this direction suggests reasonably to neglect the J_3 exchange in the model. Finally, due to the doubly-open structure there is no direct superexchange path linking Cu1 and Cu1' and consequently negligible interactions are expected. The resulting magnetic arrangement is sketched in Figure 4.15(b), with strong antiferro-magnetic interactions J_1 and J_2, of similar size, and the possibility of a small ferromagnetic interaction J_3.

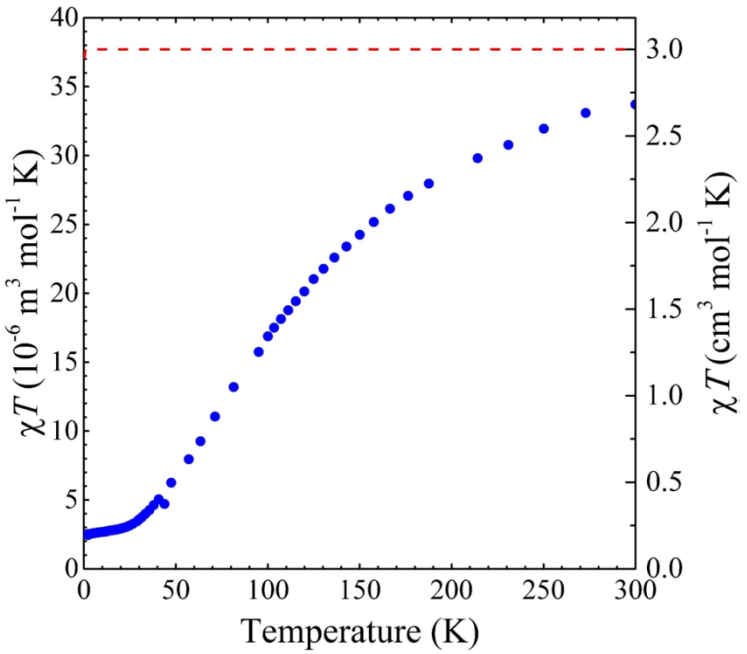

Figure 4.13. Plot of χT *vs* temperature *T* for complex 1 (χ is the linear magnetic susceptibility). The dotted line indicates a system of independent *s*=1/2 spins with a *g*-factor=2 (eight Cu^{2+} ions in asymmetric unit of complex 1). The left-hand scale is in SI units and the right-hand in CGS units.

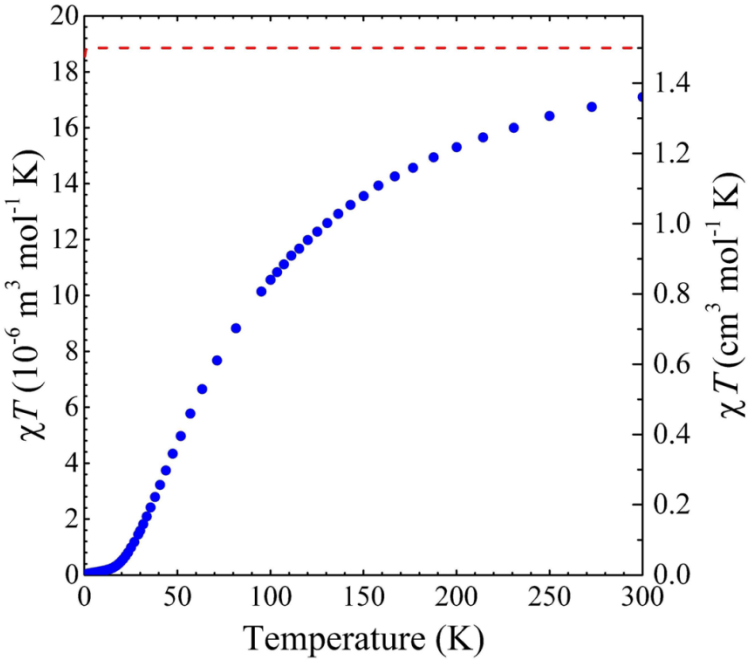

Figure 4.14. Plot of χT *vs* temperature *T* for complex 2 (χ is the linear magnetic susceptibility). The dotted line indicates a system of independent *s*=1/2 spins with a *g*-factor=2 (four Cu^{2+} ions in asymmetric unit of complex 2). The left-hand scale is in SI units and the right-hand in CGS units.

Table 4.6. Bond lengths (Å) and angles (°) for complexes 1 and 2. The *italic* entries represent cross-diagonal bonds.

Complex 1	Cu-Cu(Å)	Cu-O-Cu(Å)	Cu-O-Cu(°)
Cu_{12},Cu_{34}	3.152, 3.148	3.928,3.924	106.74,106.711
Cu_{23},Cu_{14}	3.345, 3.398	3.72, 3.91	117.247, 120.671
Cu_{13}	*3.939*	*4.954, 4.882*	*103.160,105.736*
Cu_{24}	*3.311*	*4.512,4.397*	*93.6, 97.228*
Cu_{67}, Cu_{58}	3.397, 3.327	3.882, 3.897	122.179, 117.228
Cu_{56}, Cu_{78}	3.147, 3.190	3.937, 3.947	106.109, 107.841
Cu_{57}	*3.850*	*4.96, 4.85*	*99.63,103.43*
Cu_{68}	*3.250*	*4.52, 4.40*	*90.99, 94.80*
Complex 2	**Cu-Cu(Å)**	**Cu-O-Cu(Å)**	**Cu-O-Cu(°)**
Cu_{12}, $Cu_{1'2'}$	3.191	3.940	108.137
$Cu_{12'}$, $Cu_{21'}$	3.387	3.942	118.390
$Cu_{22'}$	3.138	4.336	91.367
$Cu_{11'}$	*3.932*	*4.881*	*105.531*

Fitting experimental magnetic susceptibility data with multiple exchange pathways is not straightforward, and different models can be used.[4.26] In addition, for a given model, dependencies between the parameters lead to difficulties establishing reliable estimates for the exchange strengths and their associated errors. In this case, given the discussion above, the appropriate model should be that of a rectangular tetramer of spins as outlined in reference.[4.27] The susceptibility is given by

$$\chi(T) = 2\beta(g\mu_B)^2 \frac{5 + e^{\beta J_1} + e^{\alpha\beta J_1} + e^{(1+\alpha)\beta J_1}}{5 + 3e^{\beta J_1} + 3e^{\alpha\beta J_1} + 3e^{(1+\alpha)\beta J_1} + 2e^{(1+\alpha)\beta J_1}\cosh(f\beta J_1/2)},$$

Where $\alpha = J_2/J_1$, $\beta = 1/k_BT$, and $f = \sqrt{1 - \alpha + \alpha^2}$.[4.27]

We also include a Curie term to account for the paramagnetic upturn seen at low temperatures. As mentioned, dependencies exist between parameters in the model, and in particular multiple combinations of α and J_1 can well account for the data. Given the similarity between the J_1 and J_2 pathways we choose α=1 and fit the $\chi(T)$ data to an effective

square tetramer model. For complex **2** this yields J_1=J_2=110(1) K, g=2.07(1) with a 0.31(1) % of impurity spin contribution. The results of the model, with and without the impurity contribution, are shown in Figure 4.12.

Although the cubane-like cores of complex **1** are structurally slightly more complicated than for complex **2**, the similarities allow us to analyse the magnetism in the same way. Here a fit to the same model, shown in Figure 4.11, yields J_1=J_2=159(3) K, g=2.14(3) and a 6.50(1) % of impurity spin contribution.

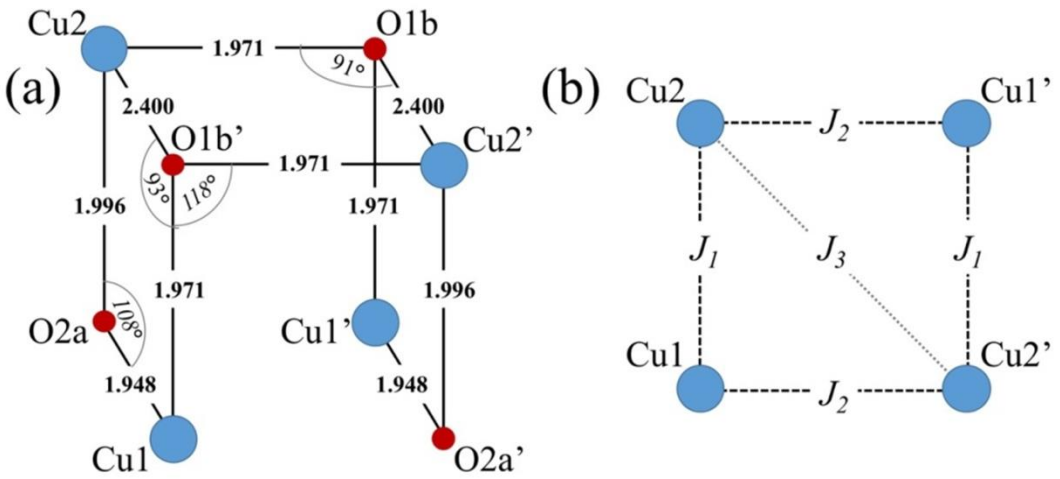

Figure 4.15. Schematic diagrams of (a) the doubly- open cubane-like structure of complex 2, and of (b) the rectangular tetramer model of antiferromagnetically coupled spins.

At the lowest temperatures the Cu ions in the cubane cores are strongly antiferromagnetically aligned and so are expected to show very little magnetization, unless the Zeeman energy due to the applied field is a significant proportion of the exchange energy. This means that at low fields the magnetization data should be dominated by the small number of paramagnetic impurities, or otherwise non-interacting spins, that are free to move in the applied field. Accordingly, for both complexes the magnetization (Figure 4.16) is found to be dominated by a Brillouin function at low fields and temperatures. The number of free spins found from these data is in good agreement with that obtained from the fits to the $\chi(T)$ data.

Magnetization data

The magnetization, as function of field, at temperatures of 1.8, 4.2 and 10 K for both complexes is shown in Figure 4.16. As explained in the main text, these data are expected to be dominated by the paramagnetic response of a small proportion of free spins. For complex **1**, the 1.8 K data are fitted very well to a Brillouin function (black line) appropriate for spin-½ paramagnetic moments. The ratio of the observed saturation field of this Brillouin function to the full saturated moment expected for the 8 Cu(II) ions contained in the asymmetric unit of unit cell is approximately 6%, in good agreement with the number of free spin-½ moments deduced from the fits to the $\chi(T)$ data. Data at higher temperature are well modelled by a Brillouin function with the same parameters as the T = 1.8 K dataset. For complex **2**, the magnetization data can be accounted for in a similar fashion by a Brillouin function, but here we must also include a small paramagnetic component, linear in applied field, that increases slightly with increasing temperature. This component presumably arises from the thermal excitation of the antiferromagnetic cubane moments, and is more noticeable in these case because of the much lower proportion of free spins and smaller value of the exchange constants as compared to complex **1**. From the Brillouin function fit for the 1.8 K data, the proportion of paramagnetic moments was estimated to be 0.1%, which is similar to the value obtained from the $\chi(T)$ data.

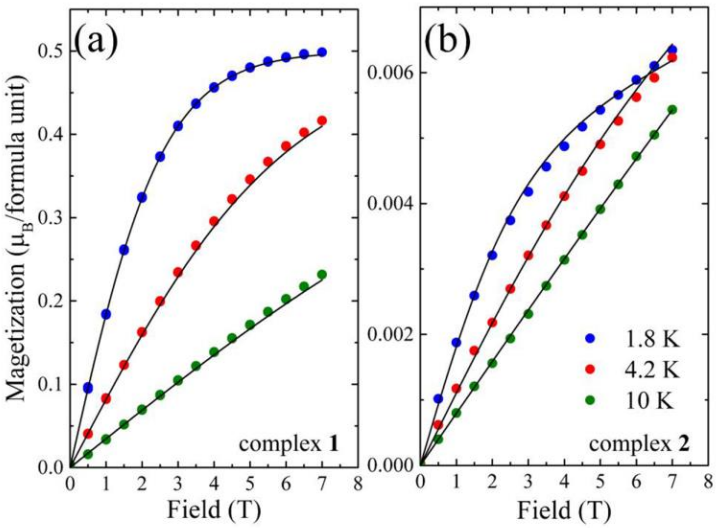

Figure 4.16. Magnetization of (a) complex 1 and (b) complex 2 at various temperatures. Circles are experimental data and lines represent the Brillouin function model described above.

4.3.5. Cyclic voltammetry studies

The cyclic voltammograms of complexes **1** and **2** were carried out in the potential range 0.0-0.6 V in methanol (ca. 1 mM), maintaining the concentration of supporting electrolyte tetraethyl ammonium perchlorate (TEAM) at 0.1 M. The cyclic voltammograms (Figure 4.17) show irreversible oxidations, at 0.422 and 0.421 V for **1** and **2**, respectively, that can be assigned as Cu^{II}/Cu^{III} oxidation process.[4.28] The values of anodic potential (E_{pa}) and anodic current (i_{pa}) are listed in Table 4.7.

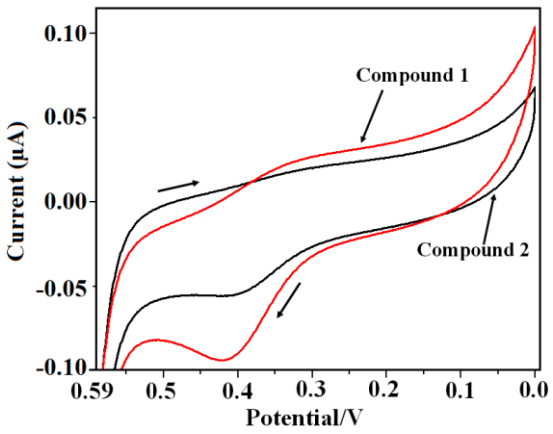

Figure 4.17. Cyclic voltammogram of complexes 1 and 2.

Table 4.7. Cyclic Voltammetric data for complexes 1 and 2.

Complex	Solvent	E_{ox} (V)[a], (i_{ac}(μA))[b]
1	Methanol	0.422, (-0.0926)
2	Methanol	0.421, (-0.0557)

[a]in methanol (supporting electrolyte NE t_4ClO_4, working electrode glassy carbon; reference electrode Ag/AgCl, scan rate 25 mV s^{-1}); [b]anodic current.

4.4. Conclusions

Here it is reported that the synthesis, structural characterization and low temperature magnetic properties of two copper(II) complexes with double open-cubane-core through the use potential tetradentate Schiff, 2-[(2-hydroxy-ethylimino)-methyl]-6-methoxy-phenol (H_2L), which is present as mono- and di-deprotonated species. The different coordination mode of this ligand give rise to discrete tetranuclear and 1D coordination polymers, the latter being achieved by bridging *p*-phenylenediacrylate anions. Both the complexes form hydrogen bonded 3D supramolecular structures. Low temperature magnetic measurements allowed to derive antiferromagnetic exchange coupling in both the complexes.